American Mineralogist, Volume 91, pages 104–110, 2006

The crystal structure of dissakisite-(La) and structural variations after annealing of radiation damage

BARBARA LAVINA,[1,*] SUSANNA CARBONIN,[1] UMBERTO RUSSO,[2] AND SIMONE TUMIATI[3]

[1]Dipartimento di Mineralogia e Petrologia, Corso Garibaldi 37, I-35137 Padova, Italy
[2]Dipartimento di Scienze Chimiche, Via Marzolo 1, I-35131 Padova, Italy
[3]Dipartimento di Scienze Chimiche e Ambientali, Via Lucini 3, I-22100 Como, Italy

ABSTRACT

The crystal chemistry of the new mineral dissakisite-(La), the Mg-analogue of allanite-(La) with ideal formula $CaLaAl_2MgSi_3O_{12}(OH)$, was studied by single-crystal X-ray diffraction and Mössbauer spectroscopy. Diffraction data indicated that it has a partially metamict state with expanded cell parameters $a = 8.959$, $b = 5.7226$, and $c = 10.232$ Å, $\beta = 115.19°$, and $V = 474.7$ Å^3. The crystal structure was refined to $R(I/\sigma(I) > 4)$ of 3.45% and $wR2$ of 8.52% (S.G. $P2_1/m$). The displacement parameters are unusually large as consistent with positional disorder. Ca and REE are partitioned between the A1 and the A2 sites, Fe^{2+} between the M3 and the A1 sites, and Fe^{3+} between the M3 and the M2 sites. Th is confined to A1. The Mössbauer spectrum implies the presence of five different iron sites, three of which are attributed to Fe^{2+} at the M3 site, one to Fe^{2+} at the A1 site, and one to Fe^{3+} at a rather distorted octahedral site.

Annealing at 700 °C caused contraction of cell edges (b and c shrank by 0.5%, a by 0.3%, β only slightly decreased; ~1% in V) and of bond distances, with a consequent overall increase in bond valences. Displacement parameters decreased by about 30%, leading to a significant increase from 1495 to 1627 in the number of reflections with $I/\sigma(I) > 4$. Structure rearrangement was achieved by means of flexible points such as the two-coordinated oxygen atoms O8 and O9, and by greater volume decreases in M3, A1, A2, and Si3 polyhedra. Si tetrahedra behaved non-rigidly, at variance with what was observed for isomorphous substitution and thermal expansion.

Despite the high Th content and the age of the mineral, the crystal structure is well preserved. The above paradox could be explained by a thermal event after formation of the mineral that reversed previous damage, or by a prolonged period under relatively high-temperature conditions.

Keywords: Crystal structure, dissakisite-(La), Mössbauer spectroscopy, new minerals, high-temperature studies

INTRODUCTION

Dissakisite-(La) was described by Tumiati et al. (2005) as a new member of the REE-rich epidote minerals, the most common of which is allanite (Gieré and Sorensen 2004). Its structure is almost identical to the structure of other (monoclinic) epidote minerals (see Franz and Liebscher 2004 for an overall review of crystal structure and chemistry). The M1 octahedra form endless, edge sharing single chains with single M3 octahedra attached on alternate sides; edge-sharing M2 octahedra form the other octahedral chain. Isolated silicon tetrahedra and corner-sharing groups of two tetrahedra cross-link the two types of octahedral chains that run parallel to [010] (Fig. 1). In allanite the A1 site is occupied by Ca and the A2 site is occupied by REE. The three octahedral M sites differ in volume and distortion. The smallest octahedral site, M2, is usually filled by Al; M1 is typically occupied by Al, Fe^{3+}, Cr^{3+}, Mn^{3+}, and Ti; the largest octahedral site, M3, is the most distorted and can accommodate trivalent and divalent cations: Fe^{2+}, Fe^{3+}, Mg, and Al. Within the structure three distinct tetrahedral sites can be identified: the isolated Si3 site and the connected Si1 and Si2 sites. Despite their different sizes the tetrahedral sites generally host only Si^{4+}. Lastly, F can substitute for O4 as in dollaseite-(Ce) (Peacor and Dunn 1988).

Dissakisite-(La) is a new member of the epidote group and has the ideal formula $CaLaAl_2MgSi_3O_{12}(OH)$. Its composition, determined by Tumiati et al. (2005) by EMP and SIMS analyses, is very complex $(Ca_{1.195}Mn_{0.009}Sr_{0.010}Na_{0.002}Th_{0.090}U_{0.003}La_{0.315}Ce_{0.262}Pr_{0.019}Nd_{0.038}Sm_{0.002}Gd_{0.001}Er_{0.001})(Al_{1.816}Mg_{0.622}Fe^{2+}_{0.244}Fe^{3+}_{0.159}Cr_{0.148}Ti_{0.030}Sc_{0.002}V_{0.008}Ga_{0.001}Ni_{0.010}Zn_{0.015})(Si_{2.970}Al_{0.022}P_{0.008})O_{11.991}F_{0.009}(OH)$ with La > Ce and relevant quantities of Th and Cr. Thus, this mineral may be defined as chromian, thorian, cerian dissakisite-(La). Dissakisite is a rare mineral. Rouse and Peacor (1993) refined dissakisite-(Ce) with composition $Ca_{1.05}(Ce_{0.57}La_{0.33}Nd_{0.07}Pr_{0.03})_{\Sigma 1.00}Mg_{0.93}Fe_{0.14}Ti_{0.06}Al_{1.91}Si_{2.94}O_{12}[(OH)_{0.94}F_{0.06}]$, while Yang and Enami (2003) described a dissakisite close to our sample in Cr and Th contents and affected by radiation damage.

Radiation damage caused by α-decay of Th and U occurs in metamict allanite. Long-term effects of this structural transformation are an increase in volume and a decrease in density. Thermal annealing of metamict minerals leads to restoration of the original crystal structure with unit-cell contraction and sharper and more intense diffraction peaks (Lima De Faria 1958; Hawthorne et al. 1991; Janeczek and Eby 1993; Paulmann et al. 2000; Paulmann and Bismayer 2001; Sokolova et al. 2004; see Gieré and Sorensen

* E-mail: barbara.lavina@unipd.it

2004 for an overall review of metamict allanites).

In this study, structural peculiarities associated with the chemical composition of dissakisite-(La) were investigated by means of single-crystal X-ray diffraction and Mössbauer spectroscopy. The significant amount of Th, the large unit-cell volume, and the high values of the displacement parameters in the untreated sample suggested that radiation damage had occurred. The sample was therefore annealed at 700 °C for 3 hours and then for a further 15 hours. The structure was refined after each annealing experiment.

Experimental methods

X-ray data collection

X-ray single-crystal data collections were performed with a four circle Stadi4-CCD diffractometer under the conditions listed in Table 1. Unit-cell parameters (Table 2) were determined in the 2θ range 10–80°. After data collection, intensities were corrected for Lorentz and polarization factors, and the absorption correction calculated using optimized shape (X-SHAPE, STOE 1999). Several fragments of the same mineral grain were tested for diffraction quality, among which DISS3, DISS5, and DISS7 were chosen for X-ray single-crystal data collections. DISS5 is the same fragment used by Tumiati et al. (2005) for complete chemical characterization by electron and ion microprobes. Lattice parameters show small differences between the three fragments. In DISS3 they are smaller than in DISS5 and DISS7, probably due to a slightly lower degree of radiation damage rather than to compositional differences. Moreover, DISS3 shows the best refinement and a considerably higher number of observed reflections (Table 2). Thus, DISS3 structural data was chosen as the most representative of the crystal structure of the dissakisite-(La).

DISS3 and DISS5 were annealed under the same conditions and showed similar behavior in both cell contraction and structural rearrangements. The crystals were sealed in a SiO_2 tube 2 mm in diameter, filled with N_2 purified with a Ti sponge heated to 800 °C, and annealed in a vertical furnace at 700 (±5) °C. Two heating experiments were performed for each crystal, for 3 hours and then for 15 hours. The crystals were quenched by dropping the sealed tube into cold water. After each annealing experiment, new X-ray data were collected under the conditions listed in Table 1.

Table 1. Summary of data collection conditions

Radiation	Mo$K\alpha$ (0.71073 Å)
Monochromator	High crystallinity graphite crystal
Collimator (mm)	0.5
2θ range	8–65°
Reciprocal space range	$-13, -8, -14 \le h,k,l \le 6, 7, 15$
Scan method	ω
Scan speed (°/s)	0.05
Temperature (°C)	23

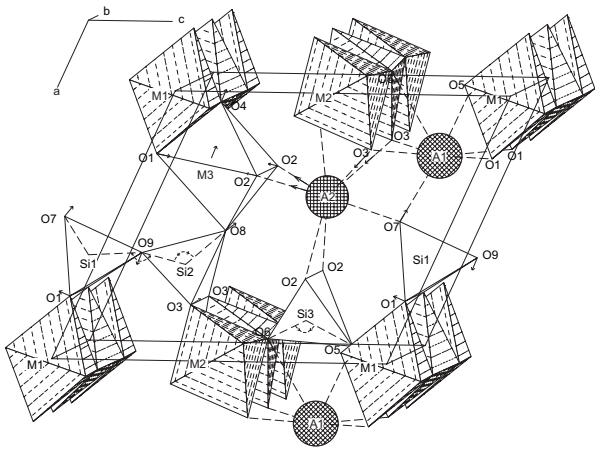

Figure 1. Projection of the structure of dissakisite-(La) viewed nearly along **b**. Only M3, Si, A2, and A1 polyhedra with centers lying at y = 1/4 are shown, to simplify drawing (hydrogen atom omitted). The arrows indicate shrinking of bond distances or changes in relative positions of atoms after annealing. The O4-M3-O8 axis shifts toward the **–a** direction, while the O8-Si2-O9 internal angle and Si1-O9-Si2 bridging angle both increase by about 1°. Shrinking of the following bond lengths is observed: M3-O1 and M3-O2; A1-O6 and A1-O7; A2-O3 and A2-O2. In the Si3 polyhedron the O5-Si3-O6 internal angle decreases (~1°) due to the approach of O6 to A1.

Structural refinement

Structural refinement was carried out against F_o^2 in space group $P2_1/m$ using the SHELX-97 program (Sheldrick 1997). The identical procedure was adopted to refine both untreated and annealed crystals. The atomic coordinates of dissakisite-(Ce) from Rouse and Peacor (1993) were taken as starting points, without considering H. No chemical constraints were imposed on the refinement. Two scattering curves were used for both A sites and only one was used for the octahedral and tetrahedral sites. At M, occupancies were not constrained to 1. Scattering curves were carefully chosen in order to obtain satisfactory agreement for F_o–F_c (table deposited). Fully ionized curves were used for A and M sites (Wilson 1992). For the tetrahedral site 0.625 occupancy of Si^{4+} against 0.375 of Si was used. For oxygen atoms a 0.50 occupancy of O^{1-} against O^{2-} (Tokonami 1965) was applied. For the A2 site the scattering curves of La^{3+} (most abundant REE) and Ca^{2+} were used (Dollase 1971). For the A1 site, only the Ca^{2+} curve was initially used. However, the determined Ca occupancy was well over 1, indicating heavier elements substituting for Ca. Th was considered the most likely substitute, because of its high atomic number and size, only slightly smaller than Ca. And indeed, Th^{4+} occupancy obtained with these two curves matched that obtained from chemical analysis. For the M2 site, only the Al^{3+} curve was adopted. In this case as well, the refined occupancy was slightly greater than 1, indicating some minor substitution by heavier elements. For the M1 and M3 sites, the dominant Al^{3+} and Mg^{2+} scattering curves were applied. Values of the refined electrons suggested significant substitutions at both sites. However, addition of a second curve (Cr^{3+} at the M1 and Fe^{2+} at the M3 sites) did not significantly change the site occupancies.

The refined parameters were: scale factors, atomic coordinates, displacement parameters (first isotropic and then anisotropic), and occupancies of A and M sites. This made a total of 123 variables in the case of the untreated sample and 124 for the annealed samples, the additional variable being the extinction factor (SHELX-97, Sheldrick 1997).

After convergence, a difference-Fourier synthesis was calculated in order to locate the hydrogen atom of the hydroxyl group. A peak of nearly equal height was regularly found after each refinement. It is however known that the hydrogen position cannot be accurately determined from X-ray diffraction data, particularly when heavy atoms are present, and no better results can be obtained (Kartashov et al. 2002). Therefore, during the last cycles, we fixed the obtained H fractional coordinates with full occupancy and set the displacement parameter at 0.05 Å^2. Values of the refined atomic coordinates for the untreated DISS3 sample are listed in Table 3.

Mössbauer spectroscopy

A Mössbauer spectrum of the sample was obtained at room temperature from untreated crystal powder (about 50 mg) in order to determine the oxidation state and coordination number of Fe. The instrument was a conventional constant-acceleration spectrometer, with a rhodium matrix ^{57}Co source (nominal strength 50 mCi). The fits were performed using a Voigt profile and a quadrupole split distribution; the isomer shift was calculated with respect to a RT α-Fe foil. Conventional constraints (component widths and areas constrained to be equal) were applied. Effects due to thickness were checked and found to be negligible.

Results

Crystal structure of the untreated sample

The lattice constants of dissakisite-(La) a = 8.959, b = 5.7226, and c = 10.232 Å; β = 115.19° (Table 2, untreated DISS3) are larger than those of dissakisite-(Ce) (a = 8.916, b = 5.700, and c = 10.140 Å; β = 114.62°; Rouse and Peacor 1993); those of DISS5 and DISS7 are even larger (see Table 2). Values of a and c for dissakisite-(La) are among the largest observed for the REE-rich epidote minerals (Gieré and Sorensen 2004). The

TABLE 2. Unit-cell parameters, refined electrons (e^-), and equivalent displacement parameters for untreated and annealed dissakisite-(La) crystals

Size (mm)	DISS3 0.15 × 0.25 × 0.25				DISS5 0.15 × 0.15 × 0.25				DISS7 0.15 × 0.15 × 0.25
	untreated	700 °C-3h	700 °C-3+15h	Δ (%)	untreated	700 °C-3h	700 °C-3+15h	Δ (%)	untreated
a (Å)	8.959(2)	8.931(1)	8.934(1)	0.3	8.972(1)	8.945(1)	8.935(1)	0.4	8.965(1)
b	5.7226(6)	5.699(1)	5.6939(8)	0.5	5.726(1)	5.7029(7)	5.7008(7)	0.4	5.730(1)
c	10.232(2)	10.182(2)	10.180(1)	0.5	10.251(1)	10.196(1)	10.190(1)	0.6	10.244(2)
β (°)	115.19(1)	115.16(1)	115.153(8)	0.0	115.29(1)	115.25(1)	115.154(9)	0.1	115.20(1)
N. refl.*	2510	3701	3840		2050	2996	3425		2532
V (Å^3)	474.7(1)	469.0(1)	468.7(1)	1.3	476.2(1)	470.4(1)	469.8(1)	1.3	476.1(1)
$R_{4\sigma}$ (%)	3.45	2.04	2.06		4.64	2.02	1.77		4.35
$N_{4\sigma}$	1495	1597	1627		1181	1305	1303		1451
R_{all} (%)	4.37	2.51	2.47		5.60	2.50	2.24		5.37
N_{all}	1853	1825	1841		1501	1507	1506		1865
wR_2 (%)	8.52	4.85	4.76		12.80	4.62	4.12		12.27
Goof	1.059	1.020	1.030		1.009	0.962	0.853		1.009
e^-_{A1}	27.98(9)	28.26(5)	28.05(5)	–0.3	28.6(2)	28.43(7)	28.52(6)	0.3	29.1(2)
e^-_{A2}	41.28(9)	41.35(5)	41.53(5)	–0.6	40.2(2)	40.10(8)	40.48(7)	–0.7	40.4(1)
e^-_{M1}	14.7(1)	14.91(6)	15.02(6)	–2.2	14.5(1)	14.78(6)	14.84(6)	–2.3	14.6(1)
e^-_{M2}	13.9(1)	13.99(6)	13.97(6)	–0.5	13.6(1)	14.01(6)	13.93(6)	–2.4	13.8(1)
e^-_{M3}	16.4(1)	16.30(6)	16.15(6)	1.5	16.3(2)	16.53(7)	16.48(6)	–1.1	16.3(1)
e^-_{tot}	114.3(2)	114.8(1)	114.7(1)	–0.4	113.2(8)	113.8(3)	114.2(3)	–0.9	114.5(6)
Displacement parameters (U_{eq}) (Å^2)									
A1	0.0205(2)	0.0144(1)	0.0140(1)	32	0.0244(3)	0.0143(1)	0.0139(1)	43	0.0218(3)
A2	0.0213(1)	0.0151(1)	0.0147(1)	31	0.0262(2)	0.0154(1)	0.0149(1)	43	0.0235(2)
M1	0.0132(4)	0.0088(2)	0.0088(2)	33	0.0176(6)	0.0093(2)	0.0092(2)	48	0.0147(5)
M2	0.0111(4)	0.0076(2)	0.0075(2)	32	0.0144(6)	0.0082(3)	0.0075(2)	48	0.0117(5)
M3	0.0177(4)	0.0115(2)	0.0103(2)	42	0.0225(6)	0.0129(3)	0.0115(2)	49	0.0198(5)
Si1	0.0113(2)	0.0079(1)	0.0075(1)	34	0.0156(4)	0.0083(2)	0.0078(2)	50	0.0123(3)
Si2	0.0131(3)	0.0089(2)	0.0085(1)	35	0.0173(4)	0.0091(2)	0.0089(2)	49	0.0143(3)
Si3	0.0105(2)	0.0069(1)	0.0068(1)	35	0.0149(4)	0.0072(2)	0.0069(2)	54	0.0116(3)
O1	0.0201(5)	0.0145(3)	0.0140(3)	30	0.0252(8)	0.0151(3)	0.0144(3)	43	0.0222(7)
O2	0.0193(5)	0.0141(3)	0.0137(3)	29	0.0249(8)	0.0150(3)	0.0143(3)	43	0.0220(6)
O3	0.0229(5)	0.0168(3)	0.0160(3)	30	0.0278(8)	0.0174(4)	0.0167(3)	40	0.0241(7)
O4	0.0159(6)	0.0114(4)	0.0110(4)	31	0.0197(10)	0.0121(5)	0.0110(4)	44	0.0169(8)
O5	0.0140(6)	0.0097(3)	0.0094(3)	33	0.0182(9)	0.0102(4)	0.0098(4)	46	0.0153(7)
O6	0.0166(7)	0.0127(4)	0.0123(4)	26	0.0221(10)	0.0133(5)	0.0123(4)	44	0.0184(8)
O7	0.0222(8)	0.0161(4)	0.0159(4)	28	0.0268(11)	0.0166(5)	0.0160(4)	40	0.0233(9)
O8	0.0364(11)	0.0289(6)	0.0282(6)	23	0.0409(15)	0.0300(7)	0.0291(6)	29	0.040(1)
O9	0.0314(10)	0.0265(5)	0.0261(5)	17	0.0355(14)	0.0271(7)	0.0262(6)	26	0.035(1)
O10	0.0178(7)	0.0124(4)	0.0120(4)	33	0.0233(11)	0.0130(5)	0.0123(4)	47	0.0194(9)

Note: Δ(%): percent variation between untreated and annealed (700 °C-3+15h) samples.
* Number of reflections used for unit-cell refinement including symmetry equivalents.

TABLE 3. Refined atomic fractional coordinates for the untreated DISS3 sample

	x	*y*	*z*
A1	0.75710(9)	3/4	0.15068(7)
A2	0.59801(5)	3/4	0.42706(4)
M1	0	0	0
M2	0	0	1/2
M3	0.2989(1)	1/4	0.2178(1)
Si1	0.3376(1)	3/4	0.0403(1)
Si2	0.6843(2)	1/4	0.2764(1)
Si3	0.1859(1)	3/4	0.3203(1)
O1	0.2334(3)	0.9910(4)	0.0322(3)
O2	0.3084(3)	0.9771(5)	0.3596(2)
O3	0.7935(3)	0.0144(4)	0.3373(3)
O4	0.0560(4)	1/4	0.1292(4)
O5	0.0456(4)	3/4	0.1475(3)
O6	0.0684(4)	3/4	0.4084(4)
O7	0.5110(4)	3/4	0.1780(4)
O8	0.5331(5)	1/4	0.3189(5)
O9	0.6188(5)	1/4	0.1006(4)
O10	0.0843(4)	1/4	0.4306(4)
H	0.159	1/4	0.305

large polyhedral volumes (Table 4), however, are not justified by the size of the occupants. On the other hand, the shortest A1-O7 bond distance is among the shortest A1-O7 bond distances in allanites, causing considerable site distortion. Atomic displacement parameters (ADPs, Table 2) for both anions and cations are very high, in particular for O8 and O9 and for A1 and A2 (cf. crystal chemical study of Bonazzi and Menchetti 1995). All these features are significant and seem to be the effects of the α-decay of Th (about 0.1 afu) as is also observed in partially metamict zircon (Murakami et al. 1991), titanite (Hawthorne et al. 1991), allanite (Janeczek and Eby 1993), and vesuvianite (Eby et al. 1993). The radioactivity of dissakisite-(La) and cracking observed in the surrounding olivine (Tumiati et al. 2005) provide further evidence for the hypothesis that the dissakisite-(La) structure has expanded due to radiation damage. On the other hand, the mineral crystallinity is still well preserved as shown by our structure refinement and by the birefringence and density (Tumiati et al. 2005). Comparison with a metamict titanite that, after annealing, showed similar decreases in ADPs and whose HRTEM images revealed only limited disruption of lattice fringes (Hawthorne et al. 1991), leads us to conclude that dissakisite-(La) occurs only with the first stage of radiation damage where aperiodic areas are not observed (Ewing and Akimoto 1994). Lastly, it is worthwhile to note the analogy between a radiation-damaged structure (expanded) and a temperature-induced one. Polyhedral volumes and ADPs of dissakisite-(La) are quite similar to those

TABLE 4. Polyhedral bond lengths (Å), selected angles (°), volumes (Å^3), mean quadratic elongation (λ), and variance (σ^2) parameters (Robinson et al. 1971) from the structure refinements

	DISS3				DISS5				DISS7
	Untreated	700 °C-3h	700 °C-3+15h	Δ (%)	Untreated	700 °C-3h	700 °C-3+15h	Δ (%)	Untreated
A1-O7	2.338(4)	2.313(2)	2.315(2)	1.0	2.342(6)	2.321(2)	2.318(2)	1.0	2.346(5)
A1-O3 ×2	2.348(3)	2.337(1)	2.337(1)	0.4	2.352(4)	2.342(2)	2.342(1)	0.4	2.352(3)
A1-O1 ×2	2.417(3)	2.413(1)	2.415(1)	0.1	2.420(4)	2.417(2)	2.417(1)	0.1	2.423(3)
A1-O5	2.598(3)	2.593(2)	2.591(2)	0.3	2.606(5)	2.597(2)	2.597(2)	0.3	2.605(4)
A1-O6	2.911(4)	2.881(2)	2.883(2)	1.0	2.914(5)	2.877(2)	2.881(2)	1.1	2.909(5)
A1-O9	[3.073(2)]	[3.057(1)]	[3.054(1)]	0.6	[3.076(2)]	[3.057(1)]	[3.055(1)]	0.7	[3.080(2)]
<A1-O>	2.482	2.469	2.470	0.5	2.487	2.473	2.473	0.6	2.487
V	19.359(3)	19.050(3)	19.073(3)	1.5	19.433(3)	19.138(3)	19.141(3)	1.5	19.480(3)
A2-O7	2.326(4)	2.319(2)	2.321(2)	0.2	2.322(5)	2.320(2)	2.323(2)	0.0	2.325(5)
A2-O2 ×2	2.519(2)	2.507(1)	2.508(1)	0.5	2.522(4)	2.510(2)	2.507(1)	0.6	2.521(3)
A2-O10	2.587(4)	2.588(2)	2.587(2)	0.0	2.590(5)	2.588(2)	2.590(2)	0.0	2.585(4)
A2-O2 ×2	2.715(3)	2.709(2)	2.707(1)	0.3	2.718(4)	2.714(2)	2.709(1)	0.3	2.717(4)
A2-O3 ×2	2.752(3)	2.733(2)	2.732(2)	0.7	2.749(4)	2.727(2)	2.730(2)	0.7	2.751(4)
A2-O8	[3.034(2)]	[3.020(1)]	[3.018(1)]	0.5	[3.040(2)]	[3.027(1)]	[3.025(1)]	0.5	[3.039(2)]
<A2-O>	2.611	2.600	2.600	0.4	2.611	2.601	2.601	0.4	2.611
V	27.932(3)	27.578(3)	27.552(3)	1.4	27.956(3)	27.612(3)	27.600(3)	1.3	27.962(3)
M1-O4 ×2	1.866(2)	1.861(1)	1.859(1)	0.4	1.869(3)	1.861(1)	1.860(1)	0.5	1.869(3)
M1-O1 ×2	1.974(2)	1.969(1)	1.972(1)	0.1	1.976(3)	1.971(1)	1.969(1)	0.4	1.975(3)
M1-O5 ×2	1.992(2)	1.982(1)	1.983(1)	0.5	1.995(3)	1.984(1)	1.982(1)	0.7	1.998(3)
<M1-O>	1.944	1.938	1.938	0.3	1.947	1.939	1.937	0.5	1.947
V	9.716(3)	9.623(3)	9.626(3)	0.9	9.766(3)	9.641(3)	9.619(3)	1.5	9.773(3)
Λ_{oct}	1.0062	1.0060	1.0060	0.0	1.0059	1.0061	1.0061	0.0	1.0060
σ^2_{oct}	16.16	15.65	15.40	4.7	15.25	15.80	15.97	−4.7	15.42
M2-O3 ×2	1.892(2)	1.886(1)	1.885(1)	0.4	1.890(4)	1.888(2)	1.888(1)	0.1	1.892(3)
M2-O10 ×2	1.892(2)	1.893(1)	1.892(1)	0.0	1.893(3)	1.893(2)	1.894(1)	−0.1	1.892(3)
M2-O6 ×2	1.947(2)	1.940(1)	1.939(1)	0.4	1.952(3)	1.944(1)	1.941(1)	0.6	1.951(3)
<M2-O>	1.910	1.906	1.905	0.3	1.912	1.908	1.907	0.3	1.912
V	9.220(3)	9.174(3)	9.157(3)	0.7	9.248(3)	9.202(3)	9.190(3)	0.6	9.241(3)
λ_{oct}	1.0054	1.0050	1.0050	0.1	1.0052	1.0049	1.0048	0.0	1.0055
σ^2_{oct}	17.79	16.06	15.98	10.2	17.01	16.16	15.93	6.3	18.17
M3-O8	1.904(5)	1.903(3)	1.906(3)	−0.1	1.895(7)	1.892(3)	1.896(3)	−0.1	1.898(6)
M3-O4	1.969(4)	1.962(2)	1.962(2)	0.3	1.970(5)	1.960(2)	1.962(2)	0.4	1.972(4)
M3-O2 ×2	2.108(3)	2.086(2)	2.084(2)	1.1	2.112(4)	2.085(2)	2.086(1)	1.2	2.117(3)
M3-O1 ×2	2.281(3)	2.262(2)	2.261(2)	0.9	2.286(4)	2.268(2)	2.266(1)	0.9	2.285(3)
<M3-O>	2.108	2.093	2.093	0.7	2.110	2.093	2.094	0.8	2.112
V	11.947(3)	11.711(3)	11.713(3)	2.0	11.985(3)	11.715(3)	11.723(3)	2.2	12.012(3)
λ_{oct}	1.0350	1.0337	1.0332	0.2	1.038	1.0337	1.0339	0.4	1.0354
σ^2_{oct}	96.25	93.82	92.80	3.6	93.93	91.97	93.23	0.7	96.45
Si1-O7	1.593(4)	1.592(2)	1.589(2)	0.2	1.597(5)	1.589(2)	1.587(2)	0.6	1.592(5)
Si1-O9	1.646(4)	1.641(2)	1.639(2)	0.2	1.650(6)	1.647(3)	1.641(2)	0.5	1.646(5)
Si1-O1 ×2	1.648(3)	1.647(1)	1.644(1)	0.4	1.648(4)	1.647(2)	1.646(1)	0.1	1.646(3)
<Si1-O>	1.633	1.630	1.628	0.3	1.636	1.632	1.630	0.4	1.632
V	2.228(2)	2.219(2)	2.209(2)	0.9	2.238(2)	2.221(2)	2.214(2)	1.1	2.226(2)
λ_{tet}	1.0029	1.0033	1.0032	0.0	1.0028	1.0033	1.0033	0.0	1.0027
σ^2_{tet}	9.83	11.17	10.87	−10.7	9.61	11.20	11.01	−14.6	9.12
Si2-O8	1.589(5)	1.589(2)	1.590(2)	−0.1	1.591(7)	1.591(3)	1.590(2)	0.1	1.593(6)
Si2-O3 ×2	1.626(3)	1.626(1)	1.625(1)	0.1	1.630(4)	1.627(2)	1.626(1)	0.2	1.628(3)
Si2-O9	1.638(4)	1.635(2)	1.637(2)	0.1	1.640(6)	1.634(2)	1.638(2)	0.1	1.646(5)
<Si2-O>	1.620	1.619	1.619	0.0	1.623	1.620	1.620	0.2	1.624
V	2.178(2)	2.175(2)	2.176(2)	0.1	2.190(2)	2.178(2)	2.177(2)	0.6	2.195(2)
λ_{tet}	1.0010	1.0012	1.0012	0.0	1.0009	1.0012	1.0013	0.0	1.0008
σ^2_{tet}	3.61	4.56	4.64	−28.5	2.93	4.66	4.74	−61.8	2.82
Si3-O2 ×2	1.637(3)	1.632(1)	1.629(1)	0.5	1.639(4)	1.633(2)	1.632(1)	0.4	1.636(3)
Si3-O6	1.652(3)	1.648(2)	1.648(2)	0.2	1.648(5)	1.649(2)	1.647(2)	0.1	1.650(4)
Si3-O5	1.677(3)	1.671(2)	1.671(2)	0.4	1.675(5)	1.671(2)	1.672(2)	0.2	1.674(4)
<Si3-O>	1.651	1.646	1.644	0.4	1.650	1.646	1.646	0.2	1.649
V	2.290(2)	2.266(2)	2.259(2)	1.4	2.288(2)	2.269(2)	2.268(2)	0.9	2.283(2)
λ_{tet}	1.0055	1.0063	1.0066	−0.1	1.0055	1.0065	1.0064	−0.1	1.0058
σ^2_{tet}	21.95	25.31	26.41	−20.3	21.96	25.96	25.49	−16.1	22.92
O5-Si3-O6	102.1(2)	101.2(1)	101.1(1)	1.0	102.3(3)	101.2(1)	101.4(1)	0.9	102.0(2)
O8-Si2-O9	110.6(3)	111.4(1)	111.4(1)	−0.7	110.2(4)	111.3(2)	111.4(1)	−1.1	110.2(3)
Si1-O9-Si2	148.7(3)	149.7(2)	150.0(2)	−0.9	148.4(4)	150.2(2)	150.3(2)	−1.3	147.8(4)

Notes: A1 and A2 sites: 7- and 8- coordination respectively with bonds <3 Å, lengths in squared brackets are not included in the calculation of the mean value. Δ(%) = percent variations of parameters between untreated and 3 + 15h annealed samples. $\lambda_{oct} = \sum_{i=1}^{6}(l_i / l_0)^2 / 6$, where l_0 is center-to-vertex distance of an octahedron with O_h symmetry, with volume equal to that of a strained or distorted octahedron with bond lengths l_i. $\lambda_{tet} = \sum_{i=1}^{4}(l_i / l_0)^2 / 4$, where l_0 is center-to-vertex distance for a tetrahedron with volume equal to that of a strained or distorted tetrahedron with bond lengths l_i. $\sigma^2_{oct} = \sum_{i=1}^{12}(\theta_i - 90°)^2 / 11$, $\sigma^2_{tet} = \sum_{i=1}^{6}(\theta_i - 109.47°)^2 / 5$.

of thermally expanded strontian piemontite (Catti et al. 1988) as if a radiation damaged structure had features comparable to a temperature-induced one.

Mössbauer data

The spectrum (Fig. 2) presents two broad and asymmetric absorption peaks due to the superposition of different Fe^{2+}

TABLE 5. Mössbauer hyperfine parameters at room temperature for untreated dissakisite-(La)

Assignment	δ (mm/s)	ΔE_Q (mm/s)	Γ (mm/s)	A (%)
Fe^{2+} A1	1.00	1.30	0.37	19
Fe^{2+} M3	1.07	1.72	0.38	25
Fe^{2+} M3	1.12	2.17	0.37	14
Fe^{2+} M3	1.18	2.80	0.29	6
Fe^{3+} M	0.33	1.58	1.01	37

types, while the larger area of the low velocity peak indicates the presence of at least one site containing Fe^{3+}. Accordingly, the spectrum was initially fitted with 5 Lorentzian doublets (4 due to Fe^{2+} and one to Fe^{3+}), which resulted in reasonable parameters. To account for the site-occupancy refinement data, suggesting the possibility of a second Fe^{3+} site, the spectrum was then fitted with the addition of a sixth component. The results showed a very small improvement in the χ^2 value and similar parameter values. Thus, a definitive choice between the two models cannot be made on the basis of the Mössbauer spectrum alone. However, the unreasonably large value of the quadrupole splitting of the second Fe^{3+} component, the large values for the linewidths, and the dependence of the results on the input data are in favor of the first solution, bearing in mind that the broad absorption due to the Fe^{3+} species can hide a second component. An attempt to fit the spectrum with a quadrupole split distribution based on the Voigt profile method did not give reliable results as one Fe^{3+} and one Fe^{2+} component systematically disappeared unless extensive use of constraints was made.

All the iron is present in octahedral coordination, although displaying various distortions due to non-ideal site geometry, different Fe-O bond distances and distributions, and nature of the next nearest neighbors. The very low values of both isomer shift and quadrupole splitting for iron at the first site (1.00 and 1.30 mm/s respectively; Table 5) place it on the borderline between octahedral and tetrahedral coordination. This may be due to the formation of very long Fe-O bonds and to the possibility of achieving high symmetry. Such evidence supports the hypothesis that this iron occupies the large A1 site, as further suggested by the 19% area, a value close to that found by cation partitioning considerations (16%). The three other different Fe^{2+} centers occupy the M3 site. The wide range of ΔE_Q values can be reasonably attributed to the second sphere cations that, being different in both type and ionic charge, cause severe imbalance in the electron density and may affect the Fe-O bond distances and O-Fe-O bond angles. The only Fe^{3+} occupies an octahedral site that is rather distorted as shown by the high quadrupole splitting value (1.58 mm/s) and extremely large linewidth (1.01 mm/s). Attempts to split this doublet or to fit it as a quadrupole splitting distribution failed because in the first case too many parameters had to be constrained to fixed values and in the second only a symmetrical, and so meaningless, Gaussian probability curve was obtained. Therefore, it was not possible to obtain any information on the Fe distribution among the three M sites from Mössbauer spectroscopy alone. Finally, a spectrum collected at low temperature (14 K) failed to provide additional useful information. Due to the small amount of remaining material the spectrum showed the presence of two broad absorptions without any details, and even the shoulder visible at the highest velocity in the RT spectrum completely disappeared inside the main band as a result of the different temperature dependences of the hyperfine parameters.

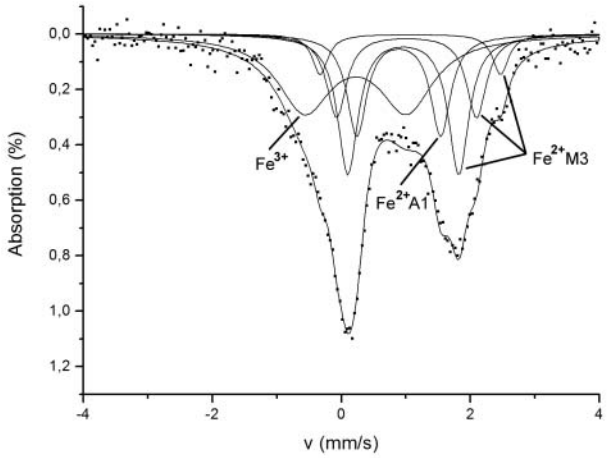

FIGURE 2. Mössbauer spectrum at room temperature for untreated dissakisite-(La)

Cation distribution

Cations were partitioned on the basis of Mössbauer spectra and refinement electrons at the A and M sites (e^-, Table 2). As previously discussed we refer to the structure refinement of DISS3 to describe dissakisite-(La). Including the data from DISS5 and DISS7 would not add substantial differences to the cation distributions.

In agreement with the experimental study of Catlos et al. (2000), the results of our refinement show a deficiency of typical A-site cations (REE, Ca, Th, Mn, U, and Na) equal to the excess (0.053 afu) of typical M-site cations (Al, Mg, Fe, Cr, Ti, Ni, and Zn). Accordingly, among these typical M-site cations, 0.053 Fe^{2+} afu was initially assigned to A1, which is approximately the same amount of Fe^{2+} attributed by Mössbauer spectroscopy to this site. Then, in order to achieve the number of refinement electrons (e^-_{A1} = 27.98), together with 0.792 afu of Ca, we filled this site with the heaviest elements: Th (0.090 afu), U (0.003 afu), Er (0.001 afu) (see Cressey and Steel 1988 for the preference of Er for the A1 site), and LREE (0.050 afu) (see also Pautov et al. 1993; Kartashov et al. 2002). The remaining Ca and LREE enter the A2 site. The following cations were assigned to the M1 site (e^-_{M1} = 14.69), together with Al: Ti (cf. Rouse and Peacor 1993), Cr (cf. Dollase 1971; Burns and Strens 1967), plus small quantities of V, Sc, and Ga. Besides Al, some Fe^{3+} was incorporated at the M2 site (e^-_{M2} = 13.91). All Mg and the remaining Fe^{2+} (as indicated by Mössbauer spectra), together with Fe^{3+}, Al, Zn, and Ni, were assigned to the largest and more distorted M3 site (e^-_{M3} = 16.44).

Thus, the resulting crystal-chemical formula is $(Ca_{0.792}Th_{0.090}Fe^{2+}_{0.053}LREE_{0.050}Mn_{0.009}U_{0.003}Na_{0.002}Er_{0.001})(Ca_{0.403}LREE_{0.595}Gd_{0.001})(Al_{0.813}Cr_{0.148}Ti_{0.030}V_{0.008}Sc_{0.002}Ga_{0.001})(Al_{0.948}Fe^{3+}_{0.052})(Mg_{0.622}Fe^{2+}_{0.192}Fe^{3+}_{0.107}Al_{0.054}Zn_{0.015}Ni_{0.010})(Si_{2.970}Al_{0.022}P_{0.008})O_{11}(O_{0.991}F_{0.009})(OH)$. Electrons from cation partitioning fit those from refinement within about 3% for each site.

Following Brown (2002) and Brese and O'Keeffe (1991), bond valences (BV) and bond valence sums (BVS) were calculated from the proposed cation distribution (Table 6). The BV calculated for

A1-O9 and A2-O8 are also reported (in square brackets), which are the two bond distances around 3 Å. However, adopting the formalism suggested by Brown (2002), A1-O9 and A2-O8 should be considered non-bonded. The BVS values are on average low compared with the formal ionic charges (Vi), thus indicating a somewhat strained structure (Brown 2002). Heat treatment, producing a shortening of most of the distances, led to slightly greater BVS values, although the discrepancies with Vi remain.

Structural changes after annealing

Structural data for the annealed DISS3 and DISS5 crystals are compared with those from the unannealed samples in Tables 2 and 4. The two crystals show similar variations except for ADPs. The DISS3 *b* and *c* lattice constants shrink by 0.5%, *a* by 0.3%, while β only slightly decreases. The volume decrease is ~1%. The refined electrons at all cation sites showed only very small variations (within 1σ) and the agreement with values obtained from cation partitioning is within about 2%, suggesting that substantial cation rearrangements or oxidation phenomena that would produce cation vacancies did not take place.

After annealing, displacement parameters showed a mean decrease of about 30% in U_{eq} values for DISS3 and of 45% for DISS5 (Table 2), becoming almost identical with those of non-metamict epidotes such as the Varenche REE-rich piemontite (Bonazzi et al. 1996). Hawthorne et al. (1991) observed that ADP reduction is correlated with the degree of metamictization in titanites. ADP reduction determined from single crystal refinements could thus be used to evaluate the extent of radiation damage in partially metamict structures where significant in-growth of aperiodic areas are not recognizable (Ewing and Akimoto 1994). Accordingly, in this study the greater reduction of ADPs in DISS5 than in DISS3 suggests that the DISS5 structure is slightly more damaged. Noticeably, the ADPs of the O8 and O9 atoms, in general the largest in the epidote structure, showed the smallest decrease (20% in DISS3 and close to 30% in DISS5). They also preserved the most remarkable anisotropy (table deposited). The overall ADP decrease caused a definite increase in the diffraction intensities, as can be seen in Figure 3, where DISS3 diffraction images projected in the $\mathbf{a}^*\mathbf{c}^*$ plane are shown before and after annealing. As a consequence, the number of reflections with $I/\sigma(I) > 4$ increased from 1495 to 1627. The increased crystallinity after annealing is also evidenced by a reduction of the refinement disagreement factors $R(I/\sigma(I) > 4)$ and *wR*2 from 3.45 to 2.06% and from 8.52 to 4.76% respectively.

Contraction in the structure was strongly anisotropic with regard to single bond lengths and angles. The M3 octahedron underwent the strongest contraction as a result of shrinking of the two longest M3-O1 and M3-O2 distances, thus becoming less distorted. For the A1 site shrinking in particular of A1-O6 and A1-O7 took place and for the A2 site of A2-O3 and of the two shortest A2-O2, with a general volume decrease of ~1.5%. Bond valences calculated after annealing showed that strain decreased and the atoms regained a more "rigid" neighborhood. In the tetrahedra, the Si3 polyhedron showed the highest contraction and distortion increase, due to the decrease in the internal angle O5-Si3-O6 (~1°), caused in turn by the approach of O6 to A1. Moreover, in accord with Dollase (1971), Catti et al. (1988), and Liebscher et al. (2002), we observed translations and rotations in the M3 polyhedron and the Si_2O_7 group, as indicated by arrows in Figure 1. The O4-M3-O8 axis shifts in the **–a** direction, decreasing the thickness of the multiple M3-M1-M3 octahedral chain in the [100] direction, while the O8-Si2-O9 internal angle and the Si1-O9-Si2 bridging angle both increase by about 1° (DISS3: from 110.6 to 111.4° and from 148.7 to 150.0°, respectively; DISS5: from 110.2 to 111.4° and from 148.4 to 150.3°, respectively).

In conclusion, topological variations observed after annealing occurred through flexible points in the structure, such as the two-coordinated O8, the corner-sharing between M3, Si2, and O9, the bridging oxygen of the Si_2O_7 group, similar to other structural changes observed in the epidote minerals (e.g., isomorphous substitutions: Dollase 1968, 1971; Carbonin and Molin 1980; Bonazzi and Menchetti 1995; Liebscher et al. 2002; and thermal expansion: Catti et al. 1988). Peculiar to the structural effects

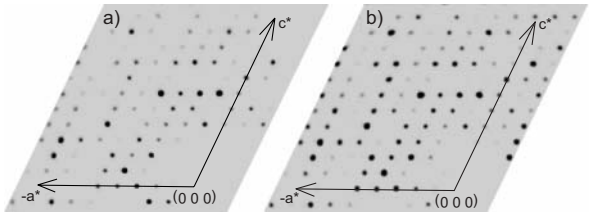

FIGURE 3. Reciprocal space reconstructions of the $\mathbf{a}^*\mathbf{c}^*$ plane: (**a**) untreated and (**b**) annealed for 3 + 15 h. The projections may be interpreted qualitatively as precession photographs (CrysAlis 169, 2002, Oxford Diffraction).

TABLE 6. Bond valences for the DISS3 untreated sample

	A1	A2	M1	M2	M3	Si1	Si2	Si3	BVS	BVS′
O1	2 × 0.32		2 × 0.44		2 × 0.21	2 × 0.94			1.91	
O2		2 × 0.31			2 × 0.33			2 × 0.97	1.80	
		2 × 0.18								
O3	2 × 0.38	2 × 0.17		2 × 0.53			2 × 0.99		2.08	
O4			2 × 0.59		0.49				1.66	
O5	0.19		2 × 0.42					0.87	1.90	
O6	0.08			2 × 0.46				0.93	1.93	
O7	0.39	0.53				1.09			2.01	
O8		[2 × 0.08]			0.58		1.10		1.68	[1.84]
O9	[2 × 0.06]					0.94	0.96		1.90	[2.02]
O10		0.26		2 × 0.53					1.32	
BVS	2.08	2.13	2.89	3.04	2.16	3.91	4.05	3.73		
BVS′	[2.20]	[2.28]								
Vi	2.24	2.59	3.03	3.00	2.12	4.00	4.00	3.98		

Notes: BVS and [BVS′]: bond valence sums calculated, respectively, without and with still appreciable bond valences for bond lengths around 3.03 Å (in square brackets). Vi: formal ion charges. Low BVS for O4 and O10 indicate hydrogen bonding as in epidotes. Tetrahedral Al distributed in Si3.

caused by radiation damage annealing is the non-rigid behavior of the Si tetrahedra, with distortion increases (Si2 and Si3) and volume decreases (Si1 and Si3).

THERMAL HISTORY AND ANNEALING OVER GEOLOGIC TIME

Given the particularly high Th content (4.3 wt% ThO_2) and the age of the mineral (~330 Ma, Tumiati et al. 2003), it is surprising that the crystal structure is still relatively well preserved, being considerably less damaged than allanites AL1 and AL2 of Janeczek and Eby (1993), which are similar in age and have a much lower Th content (about 1.5 wt% ThO_2). Annealing studies by Paulmann et al. (2000) and Paulmann and Bismayer (2001) showed that in metamict allanite the onset of recrystallization takes place at quite low temperatures: at 200 °C the structure recovers crystallinity and at 450 °C most defects are annealed after 15 min. A thermal event that occurred after formation of the mineral that reversed the previous damage may explain the above paradox. Rb-Sr cooling ages for the surrounding gneisses are up to 302 Ma for white mica (500 °C closure temperature) and up to 205 Ma for biotite (300 °C closure temperature) (Tumiati et al. 2003, and references therein). However, even assuming that radiation damage started before 205 Ma, the time would be enough to cause much greater damage of the structure than was observed. We therefore suggest either a much younger (Alpine?) heating event that annealed previous radiation damage or a much younger onset of radiation damage after a prolonged period at temperatures slightly below 300 °C (the closure temperature of biotite). The temperatures may have been lower than those achieved in the laboratory, but not to the point of producing metamorphic transformations in the host rocks or significant Rb-Sr resetting in the biotites.

ACKNOWLEDGMENTS

This work was supported by an MIUR grant (A. Della Giusta: Cofin 2001: Intracrystalline ordering-disordering process in rock-forming minerals). The authors are indebted to A. Della Giusta for help with the heating experiments and useful suggestions during the preparation of this paper. Comments and advice by reviewers G. Franz, D.R. Peacor, and A. Liebscher are gratefully acknowledged. The authors thank G. Walton, N. Whitteridge, and S. Sommacal for revising the English text.

REFERENCES CITED

Bonazzi, P. and Menchetti, S. (1995) Monoclinic members of the epidote group: effects of the $Al \leftrightarrow Fe^{3+} \leftrightarrow Fe^{2+}$ substitution and of the entry of REE^{3+}. Mineralogy and Petrology, 53, 133–153.

Bonazzi, P., Menchetti, S., and Reinecke, T. (1996) Solid solution between piemontite and androsite-(La), a new mineral of the epidote group from Andros Island, Greece. American Mineralogist, 81, 735–742.

Brese, N.E. and O'Keeffe, M. (1991) Bond-valence parameters for solids. Acta Crystallographica, B47, 192–197.

Brown, I. (2002) The Chemical Bond in Inorganic Chemistry: The Bond Valence Model, 278 p. Oxford University Press, New York.

Burns, R.G. and Strens, R.G.J. (1967) Structural interpretation of polarized absorption spectra of the Al-Fe-Mn-Cr epidotes. Mineralogical Magazine, 36, 204–226.

Carbonin, S. and Molin, G. (1980) Crystal-chemical considerations on eight metamorphic epidotes. Neues Jahrbuch für Mineralogie Monatshefte, 139, 205–215.

Catlos, E.J., Sorensen, S.S., and Harrison, T.M. (2000) Th-Pb ion-microprobe dating of allanite. American Mineralogist, 85, 633–648.

Catti, M., Ferraris, G., and Ivaldi, G. (1988) Thermal behavior of the crystal structure of strontian piemontite. American Mineralogist, 73, 1370–1376.

Cressey, G. and Steel, A.T. (1988) An EXAFS Study of Gd, Er and Lu site location in the epidote structure. Physics and Chemistry of Minerals, 15, 304–312.

CrysAlis Version 1.169.9 (release 21.05.2002) Copyright 1995-2002. Oxford Diffraction Poland Sp.

Dollase, W.A. (1968) Refinement and comparison of the structures of zoisite and clinozoisite. American Mineralogist, 53, 1882–1898.

——— (1971) Refinement of the crystal structures of epidote, allanite and hancockite. American Mineralogist, 56, 447–464.

Eby, R.K., Janeczek, J., Ewing, R.C., Ercit, T.S., Groat, L.A., Chakoumakos, B.C., Hawthorne, F.C., and Rossman, G.R. (1993) Metamict and chemically altered vesuvianite. Canadian Mineralogist, 31, 357–369.

Ewing, R.C. and Akimoto, J. (1994) The metamict state. In A.S. Marfunin, Ed., Composition, Structure, and Properties of Mineral Matter, p. 140–147. Springer-Verlag Berlin Heidelberg.

Franz, G. and Liebscher, A. (2004) Physical and chemical properties of the epidote minerals–an introduction. In A. Liebscher and G. Franz, Eds., Epidotes. Reviews in Mineralogy and Geochemistry, 56, 1–82.

Gieré, R. and Sorensen, S.S. (2004) Allanite and other REE-rich epidote group minerals. In A. Liebscher and G. Franz, Eds., Epidotes. Reviews in Mineralogy and Geochemistry, 56, 431–493.

Hawthorne, F.C., Groat, L.A., Raudsepp, M., Ball, N.A., Kimata, M., Spike, F.D., Gaba, R., Halden, N.M., Lumpkin, G.R., Ewing, R.C., Greegor, R.B., Lytle, F.W., Ercit, T.S., Rossman, G.R., Wicks, F.J., Ramik, R.A., Sherriff, B.L., Fleet, M.E., and McCammon, C. (1991) Alpha-decay damage in titanite. American Mineralogist, 76, 370–396.

Janeczek, J. and Eby, R.K. (1993) Annealing of radiation damage in allanite and gadolinite. Physics and Chemistry of Minerals, 19, 343–356.

Kartashov, P.M., Ferraris, G., Ivaldi, G., Sokolova, E., and McCammon, C. (2002) Ferriallanite-(Ce), $CaCeFe^{3+}AlFe^{2+}(SiO_4)(Si_2O_7)O(OH)$, a new member of the epidote group: description, X-ray and Mössbauer study. Canadian Mineralogist, 40, 1641–1648.

Liebscher, A., Gottschalk, M., and Franz, G. (2002) The substitution Fe^{3+}-Al and the isosymmetric displacive phase transition in synthetic zoisite: A powder X-ray and infrared spectroscopy study. American Mineralogist, 87, 909–921.

Lima De Faria, J. (1958) Heat treatment of metamict euxenites, polymignites, yttrotantalites, samarskites, pyrochlores, and allanites. Mineralogical Magazine, 31, 937–942.

Murakami, T., Chakoumakos, B.C., Ewing, R.C., Lumpkin, G.R., and Weber, W.J. (1991) Alpha-decay event damage in zircon. American Mineralogist, 76, 1510–1532.

Paulmann, C. and Bismayer, U. (2001) Anisotropic recrystallization effects in metamict allanite on isothermal annealing. In R. Gehrke, U. Krell, G. Materlik, and J.R. Schneider, Eds., HASYLAB Annual Report 2001 I: 435–436.

Paulmann, C., Schmidt, H., Kurtz, R., and Bismayer, U. (2000) Thermal recrystallization of metamict allanite on progressive and isothermal annealing. In W. Dix, T. Kracht, U. Krell, G. Materlik, and J.R. Schneider, Eds., HASYLAB Annual Report 2000 I: 625–626.

Pautov, L.A., Khvorov, P.V., Ignatenko, K.I., Sokolova, E.V., and Nadezhina, T.N. (1993) Khristovite-(Ce) (Ca, REE)REE(Mg,Fe)MnAlSi_3O_{11}(OH)(F,O), a new mineral of the epidote group. (in Russian) (abstract quoted in Mineralogical Abstracts, 45, 377, 1994).

Peacor, D.R. and Dunn, P.J. (1988) Dollaseite-(Ce) (magnesium orthite redefined): structure refinement and implications for $F + M^{2+}$ substitutions in epidote-group minerals. American Mineralogist, 73, 838–842.

Robinson, K., Gibbs, G.V., and Ribbe, P.H. (1971) Quadratic elongation: a quantitative measure of distortion in coordination polyhedra. Science, 172, 567–570.

Rouse, R.C. and Peacor, D.R. (1993) The crystal structure of dissakisite-(Ce), the Mg analogue of allanite-(Ce). Canadian Mineralogist, 31, 153–157.

Sheldrick, G.M. (1997) SHELXL-97, Program for the Refinement of Crystal Structures. University of Göttingen, Germany.

Sokolova, E., Hawthorne, F.C., Della Ventura, G., and Kartashov, P.M. (2004) Chevkinite-(Ce): crystal structure and the effect of moderate radiation-induced damage on site-occupancy refinement. Canadian Mineralogist, 42, 1013–1025.

STOE X-SHAPE, Version 1.06 (1999) Crystal Optimisation for Numerical Absorption Correction, STOE and Cie GmbH, Darmstadt.

Tokonami, M. (1965) Atomic scattering factor for O^{2-}. Acta Crystallographica, 19, 486.

Tumiati, S., Thöni, M., Nimis, P., Martin, S., and Mair, V. (2003) Mantle-crust interactions during Variscan subduction in the Eastern Alps (Nonsberg-Ulten zone): Geochronology and new petrological constraints. Earth and Planetary Science Letters, 210, 509–526.

Tumiati, S., Godard, G., Martin, S., Nimis, P., Mair, V., and Boyer, B. (2005) Dissakisite-(La) from the Ulten zone peridotite (Italian Eastern Alps): A new end-member of the epidote group. American Mineralogist, 90, 1177–1185.

Wilson, A.J.C. (1992) International Tables for Crystallography, Volume C, 883 p. Kluwer Academic Publishers, Dordrecht, The Netherlands.

Yang, J.J. and Enami, M. (2003) Chromian dissakisite-(Ce) in a garnet lherzolite from the Chinese Su-Lu UHP metamorphic terrane: implications for Cr incorporation in epidote-group minerals and recycling of REE into the Earth's mantle. American Mineralogist, 88, 604–610.

MANUSCRIPT RECEIVED MAY 25, 2004
MANUSCRIPT ACCEPTED MAY 2, 2005
MANUSCRIPT HANDLED BY JOHN AYERS